International Journal of Microwave and Wireless Technologies

cambridge.org/mrf

Charge-conservative GaN HEMT nonlinear modeling from non-isodynamic multi-bias S-parameter measurements

Gian Piero Gibiino, Alberto Santarelli and Fabio Filicori

Department Electrical, Electronic, and Information Engineering "G. Marconi" (DEI),University of Bologna, Viale Risorgimento 2 - 40136 Bologna, Italy

Research Paper

Cite this article: Gibiino GP, Santarelli A, Filicori F (2019). Charge-conservative GaN HEMT nonlinear modeling from non-isodynamic multi-bias S-parameter measurements. *International Journal of Microwave and Wireless Technologies* **11**, 431–440. https://doi.org/10.1017/S1759078719000059

Received: 16 November 2018
Revised: 30 December 2018
Accepted: 2 January 2019
First published online: 8 February 2019

Keywords:
Compact transistor modeling; empirical modeling; GaN HEMT; charge conservation

Author for correspondence:
Gian Piero Gibiino, gianpiero.gibiino@unibo.it

Abstract

Guaranteeing charge conservation of empirically extracted Gallium Nitride (GaN) High-Electron-Mobility Transistor (HEMT) models is necessary to avoid simulation issues and artifacts in the prediction. However, dispersive effects, such as thermal and charge-trapping phenomena, may compromise the model extraction flow resulting in poor model accuracy. Although GaN HEMT models should be extracted, in principle, from an isodynamic dataset, this work deals with the systematic identification of an approximate, yet most suitable, charge-conservative empirical model from standard multi-bias S-parameters, i.e., from non-isodynamic data. Results show that the obtained model maintains a reasonable accuracy in predicting both small- and large-signal behavior, while providing the benefits of charge conservation.

Introduction

As the performance requested to microwave devices develops to meet the demanding targets of the wireless industry, the need for fast and reliable design tools is ever increasing. In this framework, empirical High-Electron-Mobility Transistor (HEMT) modeling faces a number of challenges as Gallium Nitride (GaN) HEMT devices, which feature an unprecedented performance both in terms of power density as well as wideband operation [1], are introduced at an industrial level [2]. Indeed, GaN devices show inherent low-frequency (LF) dispersive effects [3] that considerably impact their radio-frequency (RF) behavior in power amplifiers [4] and RF switches [5] applications.

During the last years, modeling developments were mainly focused on the impact of LF dispersive phenomena on the conduction current [4,6–11]. Lately, attention has been drawn to the influence that charge trapping may have on the displacement current modeling flow [12], and the consequent impact on linearity performance prediction under modulated excitation, namely the prediction of intermodulation distortion (IMD) products. The description of the displacement current component involves choosing a suitable model representation, either in terms of nonlinear capacitances, as in Fig. 1(a), or by means of nonlinear charge functions, as in Fig. 1(b). Capacitive models, commonly implemented as equivalent-circuit models based on nonlinear capacitance lumped elements, are widespread for their immediate implementation and intuitive behavior. They can be described in a general way by considering a two-port capacitance matrix, whose elements can be directly extracted from small-signal measurements. Notably, implementing a model in terms of bivariate capacitances does not automatically guarantee terminal charge conservation, causing potential issues in circuit simulation [13]. In time-domain circuit analysis, non-charge-conservative models may cause time-increasing integration errors in long transient simulations. In harmonic-balance (HB) simulation, a non-physical dc current is generated. Especially at the gate port, such a spurious dc component in the presence of the large impedance usually adopted in the gate bias network, might cause large spurious dc voltage errors that will, in turn, change the device operating point, affecting simulation accuracy. Therefore, despite not being a general requirement, terminal charge conservation is a highly desirable model feature. Given a general two-port capacitance matrix representation:

$$C_M = \begin{bmatrix} C_{11} & C_{12} \\ C_{21} & C_{22} \end{bmatrix}, \tag{1}$$

where all elements depend on the controlling voltages v_1 and v_2, the two following additional constraints must be verified for terminal charge conservation [13]:

$$\frac{\partial C_{11}}{\partial v_2} = \frac{\partial C_{12}}{\partial v_1}; \quad \frac{\partial C_{22}}{\partial v_1} = \frac{\partial C_{21}}{\partial v_2}. \tag{2}$$

© Cambridge University Press and the European Microwave Association 2019

CAMBRIDGE UNIVERSITY PRESS

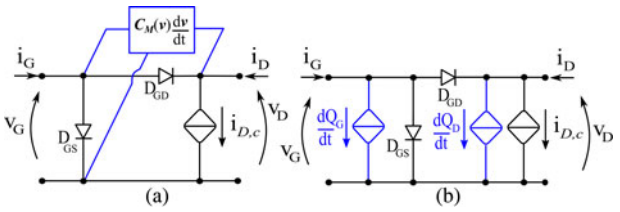


Fig. 1. (a) Intrinsic model based on the capacitance matrix. (b) Intrinsic model based on charge functions.

Conversely, a two-port charge model implementation involves identifying two charge functions. The displacement currents are obtained as time-derivatives of charge functions, so charge conservation is structural in this case.

Either choosing a capacitive or a charge representation, a fundamental aspect concerns the empirical dataset for the identification. If such a dataset consists of small-signal S-parameters and the conditions in (2) are not verified, extracting a capacitive model will involve the aforementioned simulations issues, whereas the charge functions obtained by integration will not be unique, as they will depend on the voltage-domain integration path. In fact, since multi-bias small-signal S-parameters measurements are not isodynamic, the capacitance matrix does not satisfy the condition in (2) owing to the presence of dispersive phenomena [14]. On the other hand, also an extraction from large-signal (LS) excitation typically leads to a local model approximation, unless the excitation design follows specific constraints, as will be shown in the following. Thus, maximum care should be exercised when designing the identification experiments such that (i) the operating area is properly covered; (ii) the dataset is isodynamic, i.e., all empirical values used for model extraction belong to a specific and well-defined dynamic state. With respect to the latter, LF dispersion should be particularly taken care of.

This work, by extending the contribution in [15], depicts a systematic procedure to obtain the most suitable charge-conservative GaN model that could be derived from non-isodynamic data. Such a method aims at providing fair performance prediction and the robust charge functions implementation for the many cases where special-purpose expensive setups capable to perform isodynamic experiments [16,17] are not available. The paper is organized as follows. The section "Large-signal identification for GaN" reviews the specific aspects related to GaN state dynamics and depicts an experiment for obtaining isodynamic datasets from steady-state LS measurements. In the section "Approximate modeling from non-isodynamic measurements", the approach is exploited to extract approximate charge-conservative models, whose performance is evaluated in the section "Results and discussion". Conclusions are drawn in the section "Conclusion".

Large-signal identification for GaN

GaN HEMT state dynamics

GaN dispersive effects due to thermal and charge trapping phenomena involve complex electronic mechanisms within the device, showing (i) a combination of fast charge trapping mechanisms (some in the order of less than ns) and slow de-trapping transients (up to hundreds of ms); (ii) a nonlinear dependency of such dynamic behavior on the dynamically applied voltages, resulting in a composite nonlinear dynamic global response. This causes that, for example, when measuring a static current-voltage (IV) device characteristic, each bias point belongs to different thermal and charge trapping states. Therefore, classic multi-bias S-parameters cannot constitute an isodynamic dataset for charge functions extraction [14]. Although exploiting pulsed excitation for obtaining IV characteristics at fixed thermal state is straightforward, guaranteeing isodynamic conditions for GaN devices is less simple due to charge trapping [18]. To overcome the issue, different approaches can be followed.

The work in [19] exploits the peculiar trap dynamics to modify the pulsed excitations with a double-pulse pattern, where a pre-pulse is used to stabilize the regime to a pre-conditioned trapping state. Then, multi-bias double-pulsed S-parameters obtained with such a strategy can actually constitute an isodynamic dataset for charge and capacitance extraction [20]. Alternatively, a direct way to guarantee the isodynamic property to the identification dataset consists in obtaining such a dataset from a unique LS steady-state regime [16].

Optimal tone frequency selection

A number of published works has dealt with designing efficient LS excitation for capacitance or charge functions extraction [21–25]. Exploiting the simultaneous excitation of the two ports of the device, they all aim at a dense and complete coverage of the operating v_1-v_2 voltage plane. In addition, multiple derivatives of the current with respect to the applied voltages should be sampled for each point of the v_1-v_2 voltage plane in order to identify the capacitance elements. These elements, along with the limitations of the measurement setup, help in drafting a list of desired features for the excitation. Let us consider a generic voltage-controlled N-port. Let $f_1 \ldots f_N$ be N independent tone frequencies, each of which is applied to the n-th port of the device. The generated IMD products will fall at the generic frequency $\sum_{n=1}^{N} k_n f_n$, where $0 \leq |k_n| \leq K_n$ and $\sum_{n=1}^{N} |k_n| \leq K_{max}$, K_n being the maximum harmonic order at the n-th port and K_{max} the maximum mixing order. Thus, one should consider the following signal characteristics [26]:

(i) All non-negligible (i.e., of lower mixing order, or equivalently, up to the maximum nonlinear order required) IMD products must be measurable.
(ii) Two (or more) IMD products should never fall on the same frequency bin. From a measurement perspective, they should not fall too close, so to minimize measurement inaccuracies.
(iii) The excitation should be applied in a frequency range where the displacement current component is non-negligible with respect to the conduction current.
(iv) Since the displacement current is obtained as a time-derivative of charge, $\min\{\sum_{n=1}^{N} k_n f_n\}$ must be sufficiently high, in order to reduce current integration errors.
(v) The frequency response has to be frequency-confined between the upper cut-off of the LF dispersive phenomena f_{co}^{LF} and the lower cut-off of the high-frequency (HF) non-quasi-static effects f_{co}^{HF}:

$$f_{co}^{LF} < \sum_{n=1}^{N} k_n f_n < f_{co}^{HF}. \tag{3}$$

While (i) and (ii) concern the general feasibility of the measurement and (iv) relates to the extraction procedure, (v) can constitute a stringent condition for the specific case of GaN. From these

https://doi.org/10.1017/S1759078719000059 Published online by Cambridge University Press

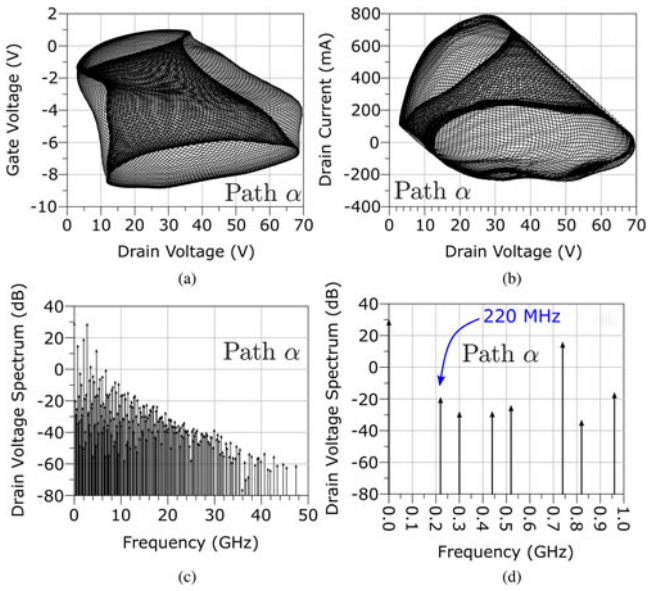


Fig. 2. Two-tone (one per port) excitation of a 0.25-μm GaN HEMT with $f_1 = 2$ GHz, $f_2 = 2.74$ GHz, $K_{1,2} = 10$, and K_{max}=20. (a) Voltage plane. (b) Drain current locus. (c) Excitation spectrum. (d) Zoom of (c) for frequencies up to 1 GHz.

specifications one realizes that, on one hand, it would be preferable to adopt a large frequency spacing between the tones, so that (ii) and (iv) would be easily satisfied. On the other hand, this is in contrast with (i) and (v) for which confining the spectral response is a must. By considering the case of a common-source transistor ($N = 2$), finding proper f_1 and f_2 will depend on a suitable value for K_{max} which, in turn, depends on the nonlinearity involved. Nevertheless, it has been shown in [26] that acceptable compromises can be found if using instrumentation with several-GHz-wide acquisition bandwidth (BW). In Fig. 2, we show the trace in the voltage plane and the drain current locus, as well as the excitation spectrum for the case of $f_1 = 2$ GHz, $f_2 = 2.74$ GHz, $K_{1,2} = 10$, and $K_{max} = 20$, determining a lower IMD at 220 MHz, well above the cut-off of the LF dispersive effects. Such an experiment can be performed by means of a Keysight PNA-X network analyzer, as shown in [16].

An interesting aspect concerns the fact that such multiple sinusoidal excitations give origin to a complex trace in the voltage domain, also known as *Lissajous curves*.[1] In this way, the voltage domain can be widely covered, and each voltage region is passed through multiple times at different speeds, depending on the ratio between the applied frequencies. This, in turn, results in different time-derivatives of the output current, ultimately leading to charge functions identification. More in detail, the resulting regime is periodic with period $T = 1/(GCD(f_1, \ldots, f_N)$, where $GCD(\cdot)$ calculates the greatest common divisor among the applied frequencies. Therefore, T is a time interval in which the traced path will return to the initial point, and it is also the minimum acquisition time for the measurement. If no greatest common divisor can be calculated, then the signal is an almost periodic multi-tone, and it will produce a trajectory that never repeats itself.

[1]More precisely, if the excitation is applied by means of signal generators with non-zero output impedance, the resulting voltage trace will consist of distorted *Lissajous curves*, depending on the nonlinearity and impedance mismatch involved.

Frequency-domain integration

The experiment depicted in the previous section results in $L \leq N$ current waveforms (L being the number of considered output ports), each of which can be depicted by an N-dimensional Fourier series:

$$i_l(\tau_1, \ldots, \tau_N) = \Re\left\{\sum_{k_1=1}^{K_1} \cdots \sum_{k_N=1}^{K_N} \bar{I}_{l,k_1,\ldots,k_N} e^{j2\pi \sum_{n=1}^{N} k_n f_n \tau_n}\right\}, \quad (4)$$

where $l = 1 \ldots L$, and $\bar{I}_{l,k_1,\ldots,k_N}$ are the Fourier coefficients relative to the current at the l-port. Given that current is the time-derivative of the charge, charge values must be obtained by integration of the displacement current, whereas the global current response in (4), in general, contains both conductive and displacement current components. This is indeed the case for the drain port of the transistor, whereas the gate port typically contains only a displacement part if the gate diodes are not turned on. The displacement current can be separated from the conduction current at the drain port by following different strategies, e.g., the one in [16].

Once any conductive part has been removed, the pure displacement currents can be integrated in the frequency domain, directly obtaining the spectral components of the charges:

$$\bar{Q}_{l,k_1,\ldots,k_K} = \frac{\bar{I}_{l,k_1,\ldots,k_N}}{j2\pi \sum_{n=1}^{N} k_n f_n}, \quad (5)$$

which can be transformed to time domain by means of the N-dimensional Fourier Series:

$$q_l(\tau_1, \ldots, \tau_N) = \Re\left\{\sum_{k_1=1}^{K_1} \cdots \sum_{k_N=1}^{K_N} \bar{Q}_{l,k_1,\ldots,k_N} e^{j2\pi \sum_{n=1}^{N} k_n f_n \tau_n}\right\}. \quad (6)$$

Obtaining the charge functions

Each of the time-domain charge loci in (6) depends on the time-domain voltage loci at all ports:

$$v_l(\tau_1, \ldots, \tau_N) = \Re\left\{\sum_{k_1=1}^{K_1} \cdots \sum_{k_N=1}^{K_N} \bar{V}_{l,k_1,\ldots,k_N} e^{j2\pi \sum_{n=1}^{N} k_n f_n \tau_n}\right\}. \quad (7)$$

If the charges constitute an exact differential in the voltage domain, the $q_l(\tau_1, \ldots, \tau_N)$ must give origin to N quasi-static functions of the $v_1, \ldots, v_n$ controlling voltages, i.e., the charge functions. Such functions, indicated with $Q_l[v_1, \ldots, v_n]$, are therefore defined by establishing an explicit correspondence between each point in the voltage domain and the respective value of waveforms q_l. If the excitation frequencies are properly defined, a sufficiently dense distribution of the traced paths in the voltage domain is obtained. In addition, the Fourier series expressions in (6) and (7) allow for any arbitrarily dense discretization of such time-domain paths. This discretization corresponds by all means to an interpolation, as the time domain signals are completely known from their frequency-domain components. In this sense, it is worth bearing in mind that the choice for the maximum harmonic

https://doi.org/10.1017/S1759078719000059 Published online by Cambridge University Press

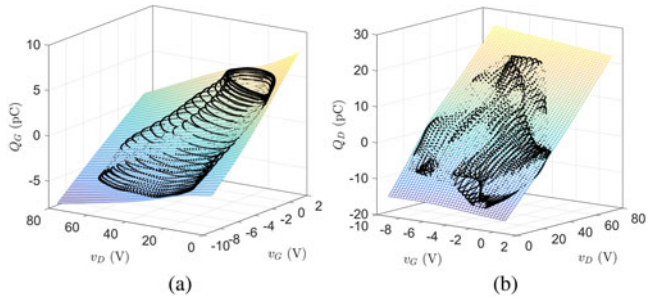


Fig. 3. Time-domain locus of the charges and relative charge functions obtained from the excitation in Fig. 2. (a) Gate charge. (b) Drain charge.

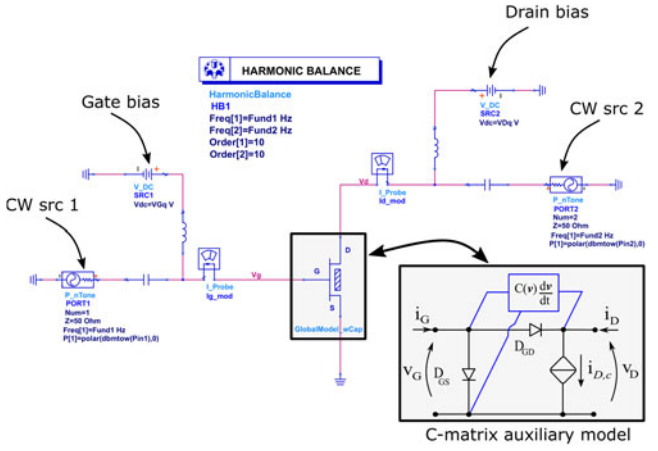


Fig. 4. Harmonic-balance simulation setup (Keysight ADS) for the implementation of the two-tone experiment.

order for each output (K_n) and the maximum IM order ($K_{\max}$) sets a limit to the nonlinearity order of the identified charge functions. In practice, the data points of q_l and v_l obtained from the discretization of (6) and (7), respectively, can be used in conjunction with suitable functions approximator algorithms, e.g., [27], to fully characterize the $Q_l[v_1, \ldots, v_n]$ functions.Let us now consider the case of a transistor in common-source configuration, which is represented as a two-port ($N = L = 2$). Figure 3 shows q_1 and q_2 loci for the gate and the drain ports, along with the identified 2-dimensional charge functions (renamed Q_G for the gate port and Q_D for the drain port). Whereas the described identification technique has been applied in [16] from LS measurements, the next section deals with the use of the same model extraction principles in conjunction with experimental datasets acquired in small-signal regime.

Approximate modeling from non-isodynamic measurements

Description of the approach

As already mentioned in the Introduction, different integration paths applied to capacitances identified from non-isodynamic measurements will generally lead to different charge functions, whereas a unique charge function per port must be implemented. On the other hand, non-isodynamic datasets such as multi-bias S-parameters contain a great amount of information on the dynamics involved, as the IMD prediction of models based on capacitance matrix shows [7]. Therefore, it is worth investigating the extraction of such valuable information to obtain optimal charge functions from a suboptimal dataset, maintaining the prediction capabilities. In this sense, selecting the most appropriate integration path becomes a critical step.

The strategy proposed in this work consists in exciting, by simulation, a non-charge-conservative transistor model obtained from a non-isodynamic dataset in a suitable way. This allows to condition the extraction to be coherent with respect to the intended application, employing all the principles described in the section "Large-signal identification for GaN" for limiting the BW of the excitation to the range where displacement currents give the most important contribution. Finally, this also indirectly sets a suitable integration path that efficiently sweeps the operating area within the experimental dataset. The proposed procedure consists of the following steps:

(i) Perform conventional multi-bias S-parameter measurements on a dense grid of bias voltages and over a suitable frequency range where displacement currents arise. These measurements require exciting only a small-signal regime and they are normally obtained by means of a Vector Network Analyzer (VNA), typically present in any microwave laboratory.

(ii) De-embed parasitics [28], extract the capacitance matrix of the model in Fig. 1(a) from the Y-parameters, and implement the network in the schematic circuit of an HB simulator. The capacitive matrix can be simply implemented by means of a Look-Up Table (LUT), as in [7]. The conduction current can be extracted in an independent way. In this work, we have used the conduction current model in [29], while the thermal model consists of a thermal resistance ($R_\theta \simeq 13°\mathrm{C/W}$) obtained with the method in [30].

(iii) Setup an HB simulation of the implemented circuit to perform a two-tone simulation experiment (Fig. 4), where the excitation frequencies should be selected by following the indications of the section "Optimal tone frequency selection". This simulation provides, as an output, wideband spectra of the voltages and currents at the device ports, which can be transformed in time domain to evaluate the actual paths traced on the device characteristics. It should be noted that, despite such a non-charge-conservative model will generate a non-physical dc component of the current, this component is automatically discarded in the analysis.

(iv) Extract the charge functions by means of the procedure in the section "Obtaining the charge functions". Since the extraction relies, in general, on non-isodynamic data, the time-domain charge loci may not represent a sampling of a quasi-static function of the voltages, showing hysteresis. Moreover, spurious memory effects may arise due to the restricted BW deriving from the practically-limited mixing order. In this sense, a function approximator [27] that best fits the available data is necessary. In Fig. 5, the differences are shown between the actual loci of the charges (black) and the points on the approximated surface (red) for the case of a simulation experiment (excitations as from Fig. 2).

Description of the simulation experiments

To test the approach, various simulation experiments have been configured. By selecting different excitations at the two ports, different shapes and temporization of the paths traced in the controlling voltage domain are synthesized, so that different probings

https://doi.org/10.1017/S1759078719000059 Published online by Cambridge University Press

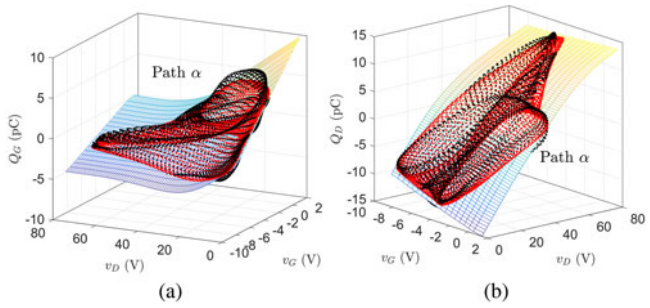


Fig. 5. Charge function fitting from the time domain charge locus (black) traced by path α. In red, the projection of the locus on the actual approximated charge surface. (a) Gate charge. (b) Drain charge.

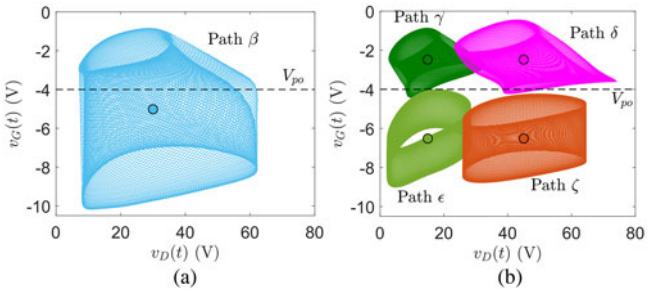


Fig. 6. Paths generated in the voltage plane. (a) Excitation β. (b) Excitations γ, δ, ϵ, and ζ.

Table 1. Integration paths for different excitation amplitudes

Path	P_1 (dBm)	P_2 (dBm)	min{v_G} (V)	max{v_D} (V)
α	12	36	− 8.1	79
β	16	33	− 10.1	62
γ	7	30	− 4.3	32
δ	9	30	− 4.2	73
ϵ	5	27	− 9	28
ζ	8	30	− 8.8	65

Table 2. Integration paths for different frequencies

Path	f_1 (GHz)	f_2 (GHz)	f_2/f_1	min{f} (MHz)	max{f} (GHz)
α	2	2.74	1.37	220	47.4
η	1	1.37	1.37	110	23.7
θ	0.5	0.685	1.37	55	11.85
ι	2	2.54	1.27	160	45.4
κ	2	2.94	1.47	120	49.4

of the device response can be evaluated. Given that the capacitance-based model obtained from S-parameters measurements is not charge conservative, such different excitations lead, in general, to the identification of different charge functions. Therefore, these tests allow to quantify such differences and estimate how much this suboptimal extraction dataset will affect the accuracy of the model.

As a preliminary step, the S-parameters of a 8× 125, 0.25-μm GaN-on-SiC HEMT were measured from 100 MHz up to 30 GHz by means of an 8510 Keysight VNA. A standard *RLC* π-network of extrinsic parasitic elements was extracted by means of the method in [28] ($R_G = 0.9\ \Omega$, $R_D = 1.6\ \Omega$, $R_S = 0\ \Omega$; $L_G = 140$ pH, $L_D = 104$ pH, $L_S = 8$ pH, $C_{GS} = 28$ fF, $C_{DS} = 65$ fF, $C_{GD} = 0$ fF). The capacitance elements extracted from the de-embedded measurements have been implemented in the auxiliary capacitive model of Fig. 1(a) and the schematic of Fig. 4. Then, different sinusoidal excitations[2] were applied in the simulations for obtaining:

(i) Different operating areas. These can be configured by selecting different bias points and different amplitudes for the excitations signals. In this work, we have configured six different excitations α to ζ, whose parameters are reported in Table 1. While the shape of the α path was already provided in Fig. 2, the others are reported in Fig. 6, showing the different coverages of voltage domain, both above and below the pinch-off voltage V_{po} of the device.

(ii) Different excitation frequencies. These can influence both the shape of the synthesized path, as well as the speed rate at which the path is passed through. In particular, the shape of the path depends on the ratio between the two excitation frequencies. The applied excitations and the resulting paths (η to κ) are reported in Table 2, while the amplitude levels of the excitations are kept the same as the ones for α. The paths η and θ maintain the same frequency ratio as α, so the shape of the path remains the same, while the speed at which this is passed through is 2 × slower for η ($T = 100$ ns) and 4 × slower for θ ($T = 200$ ns). Such temporization differences can be clearly seen in the frequency domain, as shown in Figs 7(a) and 7(b). For ι and κ, the frequency ratio is changed, so that the traced paths change, as shown in Fig. 8.

[2]For all cases, $k_{1,2} = 10$ and $K_{\max}$=20.

Results and discussion

Charge functions approximation

After the dynamic voltage and currents are saved for the α to κ configurations depicted in the previous section, two time-domain charge waveforms q_G and q_D (for gate and drain) are extracted for each case by integrating the displacement currents in frequency domain. Then, these are fitted to two 2-dimensional surfaces in the v_G-v_D variables. Given that some of the synthesized loci do not cover the full operating area in the voltage plane, the resulting charge functions will only be evaluated within the respective limited domain. An interesting metric to consider is the fitting relative error to the surface E_F:

$$\mathrm{E}_F = \frac{\int_T \left\{ Q[v_G(t), v_D(t)] - q(t) \right\}^2 dt}{\int_T q(t)^2 dt}, \tag{8}$$

where $Q[v_G(t), v_D(t)]$ is the approximated charge surface, $q(t)$ is the time-domain charge locus, and T is the period of the excitation. If all the values of $q_G(t)$ and $q_D(t)$ were perfectly laying on a surface, such fitting error would be zero. Conversely, the presence

https://doi.org/10.1017/S1759078719000059 Published online by Cambridge University Press

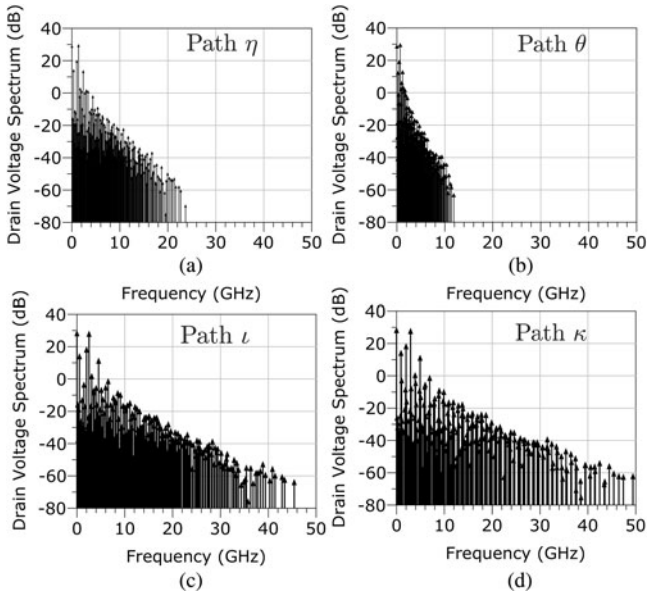


Fig. 7. Spectrum response for the paths η, θ, ι, and κ.

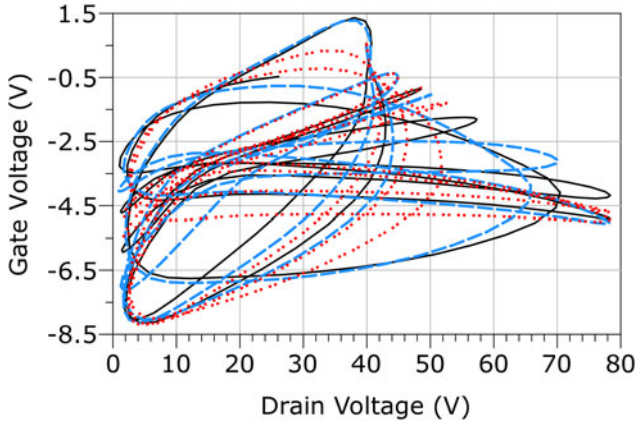


Fig. 8. Paths α (black solid line), ι (blue long dash), and κ (red dot) in the voltage plane for an observation time of 2.5 ns.

of a fitting error means that the sampled charge data points do not perfectly belong to a quasi-static function of the applied voltages. Therefore, this indicates that such sampled charges depend on the traced path, due to the different dynamic states at which the S-parameter dataset was acquired.

The fitting error for the different excitations used in this work is shown in Fig. 9. It can be seen that, for all paths, a certain fitting relative error up to 12% is present, and that such an error is generally larger for Q_G with respect to Q_D. Notably, the error is lower for the β, γ, ϵ, and ζ paths, which are obtained either by biasing the device below pinch-off, or at relatively low drain voltage for γ (i.e., in zero or low-power dissipation conditions). This aspect seems in agreement with the general principle for which operating temperature and trap state differences, particularly evident for high quiescent voltages and currents, will change the state of the device, thus making the multi-bias S-parameters non-isodynamic.

It is worth noting that a small surface fitting error does not directly mean that a unique charge function has been obtained from different excitation conditions. In fact, the different paths

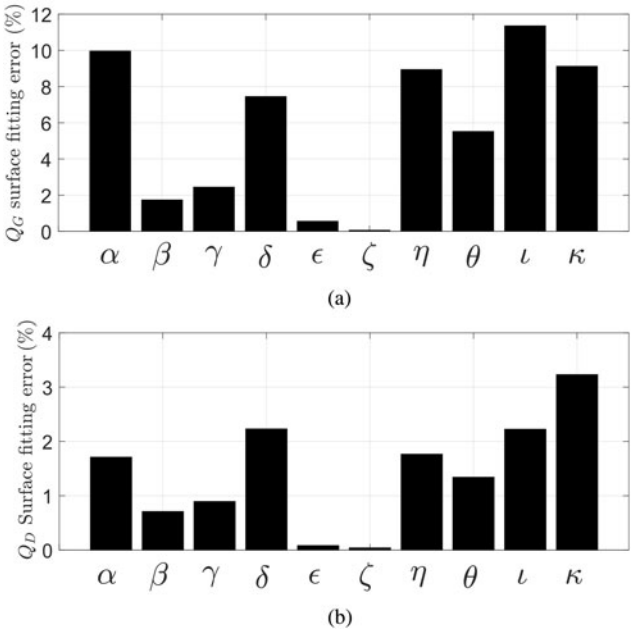


Fig. 9. (a) Gate charge surface fitting error (%). (b) Drain charge surface fitting error (%).

could generate charge signals laying on different surfaces. To clarify this aspect, the following relative error between the approximated charges has been calculated:

$$\mathrm{E}_Q = \frac{\int\int_{D_v}\left\{Q[v_G, v_D] - \hat{Q}[v_G, v_D]\right\}^2 dv_G dv_D}{\int\int_{D_v}\hat{Q}[v_G, v_D]^2 dv_G dv_D}, \tag{9}$$

where $\hat{Q}[v_G, v_D]$ is a reference charge function and D_v is the voltage domain corresponding to each path. The resulting values of E_Q are shown in Fig. 10. For the charge functions obtained by biasing the HEMT in the ON-state, i.e., γ, δ, η, θ, ι, and κ, the chosen reference charge functions are the ones extracted by the configuration α. For the charge functions obtained by biasing below pinch-off, i.e., ϵ and ζ, the reference charge functions are the ones obtained with the configuration β.

It can be noted that the gate charge function obtained from δ reports more than 15% in relative error with respect to α. This means that the fitting error shown in Fig. 9 has caused the synthesis of two different charge models. On the other hand, despite the gate charges from paths η to κ (as well as α) were showing substantial fitting error, the approximated charge models they provide are quite similar to each other, originating only up to $\sim$ 2% of relative error. Apart from the gate charge from δ, the different charge models only show a few percent of relative error. This means that, despite having been obtained from different excitations of a non-isodynamic dataset, they are relatively similar to each other.

Small-signal behavior

In order to evaluate their prediction capabilities, the charge functions have been implemented in CAD (Keysight ADS), giving origin to ten different charge models. Such implementations take advantage of the Symbolically-Defined Device (SDD) component,

https://doi.org/10.1017/S1759078719000059 Published online by Cambridge University Press

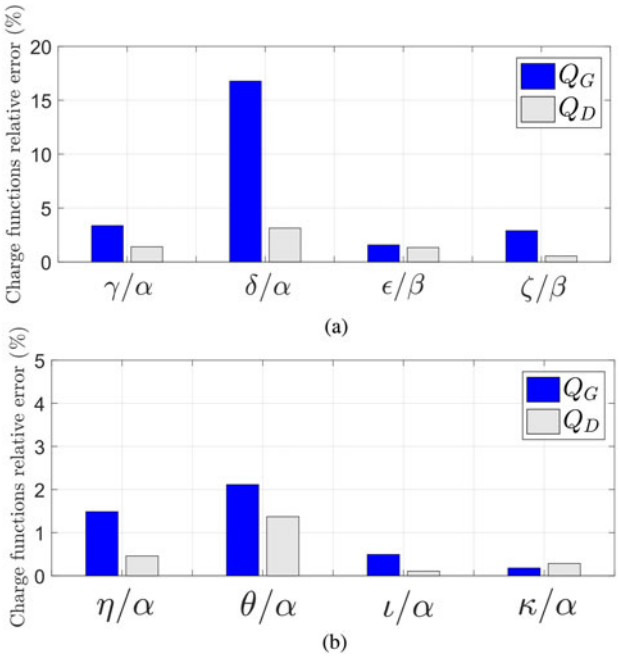


Fig. 10. (a) Relative errors of the charge functions obtained for paths γ, δ (referred to the ones obtained from path α), ϵ, ζ (referred to the ones obtained from path β). (b) Relative errors of the charge functions obtained for paths η, θ, ι, κ (referred to the ones obtained from path α).

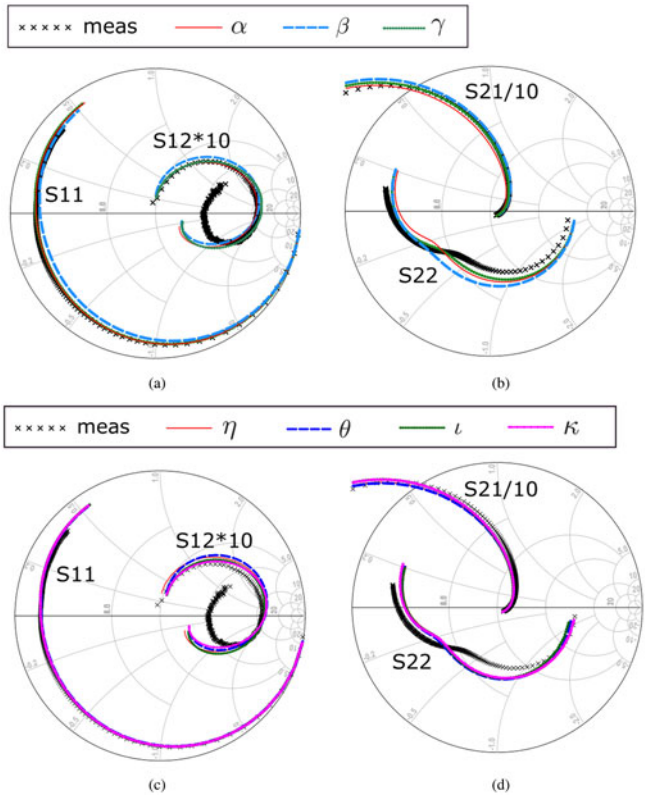


Fig. 11. Comparison between simulated and measured S-parameters at ON-state bias point $V_{GQ} = -3$ V, $V_{DQ} = 15$ V for $f = [0.1\ 30]$ GHz. (a)–(b) S-parameters obtained with models derived from paths α, β, γ. (c)–(d) S-parameters obtained with models derived from paths η, θ, ι, κ.

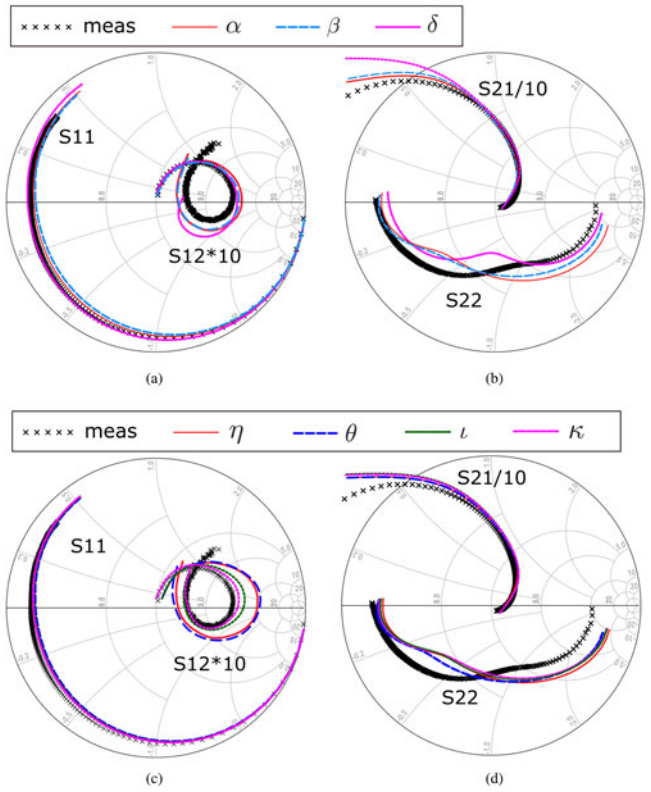


Fig. 12. Comparison between simulated and measured S-parameters at ON-state bias point $V_{GQ} = -3$ V, $V_{DQ} = 30$ V for $f = [0.1, 30]$ GHz. (a)–(b) S-parameters obtained with models derived from paths α, β, δ. (c)–(d) S-parameters obtained with models derived from paths η, θ, ι, κ.

which allows to calculate the derivatives of the quantities applied to its terminals. Considering HB simulations, this corresponds to a multiplication by frequency at each frequency. Then, once the derivatives are obtained in the frequency domain, they can be transformed to time domain. In the specific case, the charge functions covering a suitable operating area are read from LUTs. Then, the output of the LUTs is directly applied to the SDD for obtaining the corresponding displacement currents. Alternatively, it would be possible to synthesize conventional equivalent-circuit model topologies from the same identified charge functions.

As a first test, such newly obtained models have been simulated to extract the S-parameters at different bias points. These simulations, performed in the [0.1,30] GHz range, have been compared to the actual S-parameters measurements, and are shown in Figs. 11–13. In particular, three bias points have been considered: $(V_{GQ},\ V_{DQ}) = (-3,\ 15)$ V (Fig. 11), $(V_{GQ},\ V_{DQ}) = (-3,\ 30)$ V (Fig. 12), both in the ON-state, and $(V_{GQ},\ V_{DQ}) = (-6,\ 30)$ V (Fig. 13) in pinch-off. Despite the relative differences between the charge functions obtained, the S-parameters predicted by the models are fairly similar to the measurements. In particular, it can be noted that the S_{11} is well predicted in all conditions. In the ON-state conditions, the S_{21} is fairly aligned for the $V_{DQ} = 15$ V, whereas it shows larger errors for $V_{DQ} = 30$ V. In fact, despite the model extraction derives from the very same S-parameter measurements, and although charge should not be affected by LF dispersion [16], it should be noted that the model identification is based on the LS evaluation of the measured non-isodynamic dataset, introducing spurious deviations. Therefore, as it was already mentioned concerning the fitting

https://doi.org/10.1017/S1759078719000059 Published online by Cambridge University Press

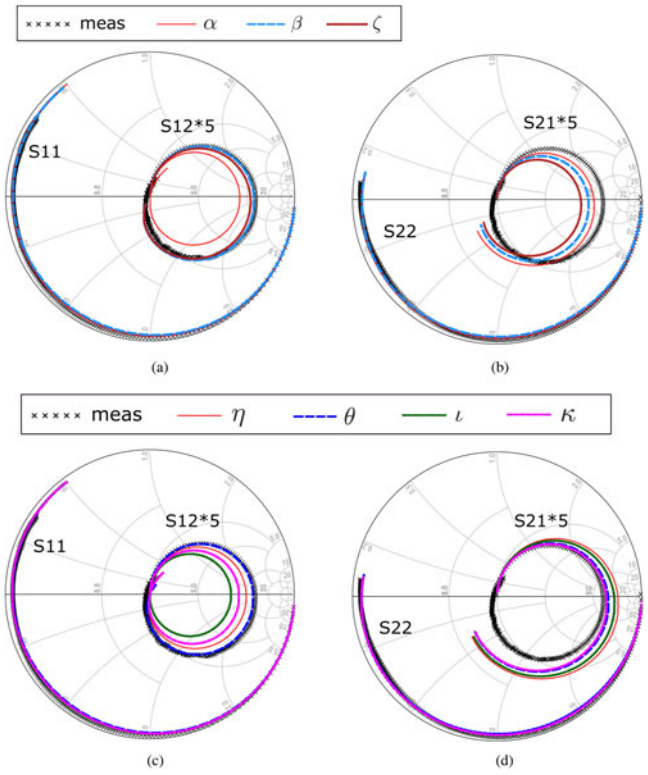


Fig. 13. Comparison between simulated and measured S-parameters at OFF-state bias point $V_{GQ} = -6$ V, $V_{DQ} = 30$ V for $f = [0.1, 30]$ GHz. (a)–(b) S-parameters obtained with models derived from paths α, β, ζ. (c)–(d) S-parameters obtained with models derived from paths η, θ, ι, κ.

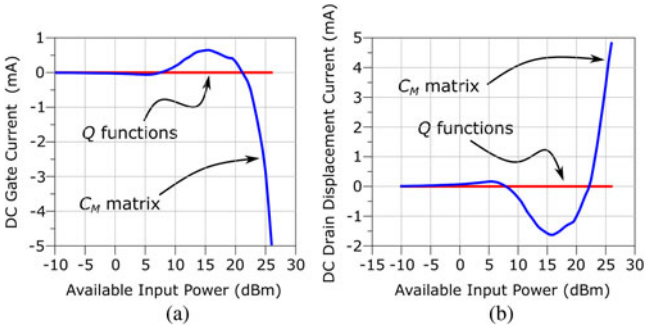


Fig. 14. Comparison between the α charge-based (charge-conservative) and the capacitance-based (non-charge-conservative) dc current model response (diodes bypassed) for a single-tone excitation at 5.5 GHz up to 4-dB gain compression, with $(V_{GQ}, V_{DQ}) = (-3.4, 30)$ V, corresponding to $I_{DQ} \simeq 60$ mA. (a) Gate current. (b) Displacement part of the drain current.

error of the δ gate charge, the prediction errors are likely to be larger in those areas where LF dispersion particularly manifests itself, i.e., at higher drain voltages. Thus, the most pronounced differences can be seen at $V_{DQ} = 30$ V for S_{22}, being S_{22} the most susceptible parameter with respect to thermal and trapping effects. Conversely, all the S-parameters are adequately reproduced when biasing in pinch-off, despite some minor disagreements in S_{12} and S_{21} among the various models.

Large-signal behavior

Figure 14 shows the prediction of the dc current by the capacitance-based model in comparison with the charge-based model

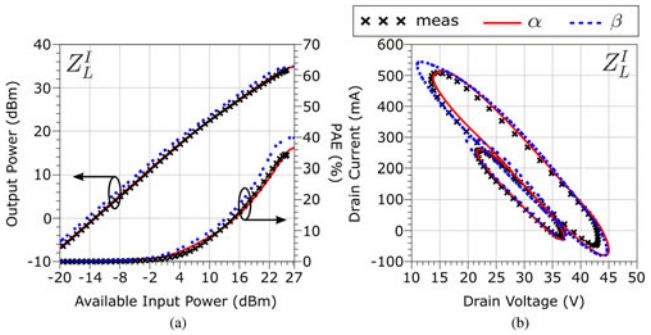


Fig. 15. (a) Prediction of RF output power and power-added efficiency (PAE) for the models extracted from the α and β paths in the presence of an RF CW at 5.5 GHz and load $Z_L^I \simeq 50\ \Omega$ (harmonics: $Z_{L,1}^I = 54 + j14$, $Z_{L,2}^I = 53 + j19$, $Z_{L,3}^I = 38 + j10$). (b) Loadline prediction for two RF input levels: 16 and 24 dBm.

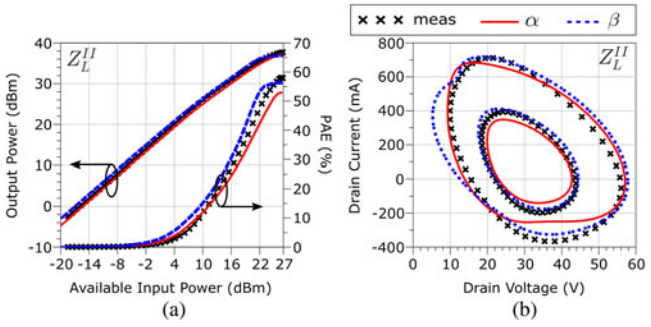


Fig. 16. (a) Prediction of RF output power and power-added efficiency (PAE) for the models extracted from the α and β paths in the presence of an RF CW at 5.5 GHz and load Z_L^{II} for maximum output power (harmonics: $Z_{L,1}^{II} = 19 + j38$, $Z_{L,2}^{II} = 89 + j89$, $Z_{L,3}^{II} = 29 + j46$). (b) Loadline prediction for two RF input levels: 16 and 24 dBm.

(obtained from path α) for a continuous wave (CW) excitation at 5.5 GHz. It can be seen that the newly implemented charge-based model do not produce any non-physical dc current, whereas the capacitance model is likely to suffer from the simulation issues discussed in the Introduction.

Two loading conditions are considered for the LS validation: $Z_L^I \simeq 50\ \Omega$, with harmonics $Z_{L,1}^I = 54 + j14$, $Z_{L,2}^I = 53 + j19$, $Z_{L,3}^I = 38 + j10$, and Z_L^{II} (maximum RF output power), with harmonics $Z_{L,1}^{II} = 19 + j38$, $Z_{L,2}^{II} = 89 + j89$, $Z_{L,3}^{II} = 29 + j46$. Figures 15–17 show the α and β model performance in the presence of an RF CW excitation at 5.5 GHz. For all tests, the chosen quiescent point is $(V_{GQ}, V_{DQ}) = (-3.4, 30)$ V, corresponding to $I_{DQ} \simeq 60$ mA. The obtained results confirm good prediction capabilities for both loads, in terms of RF output power, power-added efficiency (PAE), as well as for the IV waveforms. The CW performance for the models extracted from η, θ, ι and κ (not shown) is basically the same as for the α model.

As a last test, the charge-based models have been excited by a standard two-tone excitation (both applied at the same port) in order to characterize the in-band 3rd order IMD products (IM3) for the Z_L^{II} load. As can be seen from Fig. 18, all results provide reasonable predictions, despite some slight variations among the different model implementations.

Conclusion

In this work, we have described a method to obtain a GaN HEMT charge-conservative model from classic S-parameters

https://doi.org/10.1017/S1759078719000059 Published online by Cambridge University Press

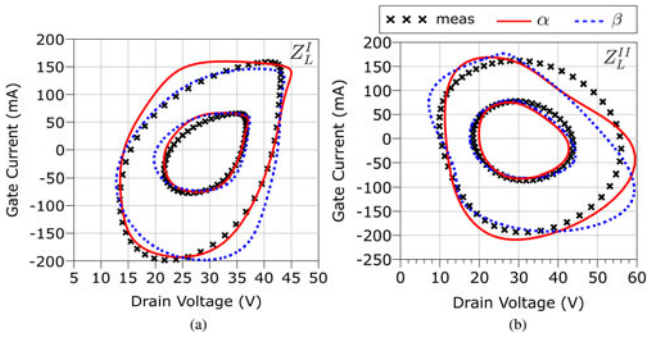


Fig. 17. Gate current prediction for the α and β models in the presence of a CW excitation at 5.5 GHz and RF input levels 16 and 24 dBm. (a) $Z_L^I \simeq 50\,\Omega$. (b) Z_L^{II} for maximum RF output power.

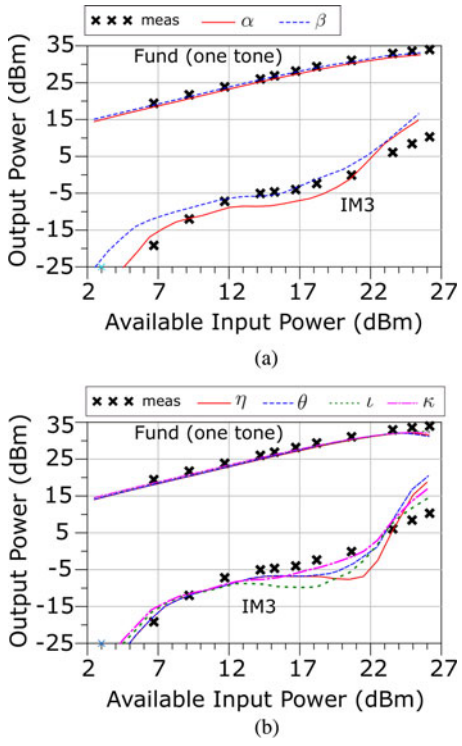


Fig. 18. Prediction of the third-order intermodulation distortion products by using the different charge functions models ($\Delta f = 20$ MHz around 5.5 GHz.) with Z_L^{II} load for maximum RF output power. (a) Prediction with models from paths α and β. (b) Predictions with models from paths η, θ, ι, and κ.

measurements, thus avoiding the use of custom setups for isodynamic acquisitions. The proposed procedure involves simulating an auxiliary capacitive model with suitable two-tone excitations, resulting in a charge functions formulation that is charge-conservative by definition. Such obtained model could then be possibly mapped into equivalent-circuit topologies that still maintain terminal charge conservation. The small- and large-signal validations show that, despite some differences in the performance with respect to measurements, the obtained models provide good prediction consistency and a robust CAD implementation.

Author ORCIDs. Gian Piero Gibiino, 0000-0002-1261-9527.

References

1. **Schuh P, Sledzik H, Reber R, Widmer K, Oppermann M, Mußer M, Seelmann-Eggebert M and Kiefer R**. (2010) GaN-based amplifiers for wideband applications. *International Journal of Microwave and Wireless Technologies* **2**, 135–141.
2. **Blanck H, Thorpe JR, Behtash R, Splettstößer J, Brückner P, Heckmann S, Jung H, Riepe K, Bourgeois F, Hosch M, Köhn D, Stieglauer H, Floriot D, Lambert B, Favede L, Ouarch Z and Camiade M**. (2010) Industrial GaN FET technology. *International Journal of Microwave and Wireless Technologies* **2**, 21–32.
3. **Santarelli A, Cignani R, Gibiino GP, Niessen D, Traverso PA, Florian C, Lanzieri C, Nanni A, Schreurs D and Filicori F**. (2013) Nonlinear charge trapping effects on pulsed I/V characteristics of GaN FETs. European Microwave Integrated Circuits Conference, 404–407.
4. **King JB and Brazil TJ** (2013) Nonlinear electrothermal GaN HEMT model applied to high-efficiency power amplifier design. *IEEE Transactions on Microwave Theory and Techniques* **61**, 444–454.
5. **Florian C, Gibiino GP and Santarelli A** (2018) Characterization and modeling of RF GaN switches accounting for trap-induced degradation under operating regimes. *IEEE Transactions on Microwave Theory and Techniques* **66**, 5491–5500.
6. **Avolio G, Schreurs D, Raffo A, Crupi G, Angelov I, Vannini G and Nauwelaers B**. (2011) Identification technique of FET model based on vector nonlinear measurements. *Electronics Letters* **47**, 1323–1324.
7. **Santarelli A, Niessen D, Cignani R, Gibiino GP, Traverso PA, Florian C, Schreurs D and Filicori F**. (2014) GaN FET nonlinear modeling based on double pulse *I/V* characteristics. *IEEE Transactions on Microwave Theory and Techniques* **62**, 3262–3273.
8. **Nunes LC, Gomes JM, Cabral PM and Pedro JC** (2015) A new nonlinear model extraction methodology for GaN HEMTs subject to trapping effects. IEEE MTT-S International Microwave Symposium (IMS), 1–4.
9. **Potier C, Jacquet JC, Dua C, Martin A, Campovecchio M, Oualli M, Jardel O, Piotrowicz S, Laurent S, Aubry R, Patard O, Gamarra P, di Forte-Poisson MA, Delage SL and Quéré R**. (2015) Highlighting trapping phenomena in microwave GaN HEMTs by low-frequency S-parameters. *International Journal of Microwave and Wireless Technologies* **7**, 287–296.
10. **Benvegnù A, Bisi D, Laurent S, Meneghini M, Meneghesso G, Barataud D, Zanoni E and Quere R**. (2016) Drain current transient and low-frequency dispersion characterizations in AlGaN/GaN HEMTs. *International Journal of Microwave and Wireless Technologies* **8**, 663–672.
11. **Xu J, Jones R, Harris SA, Nielsen T and Root DE** (2014) Dynamic FET model - DynaFET - for GaN transistors from NVNA active source injection measurements. IEEE MTT-S International Microwave Symppsium (IMS), 1–3.
12. **Wilson C and King J** (2018) Ensuring Charge Conservation in GaN HEMT Large Signal Model. European Microwave Integrated Circuits Conference (EuMIC), 61–64.
13. **Rudolph M, Fager C and Root DE** (2011) *Nonlinear Transistor Model Parameter Extraction Techniques*. Chapter 5. Cambridge: Cambridge University Press.
14. **Zucchelli G, Santarelli A, Raffo A, Vannini G and Filicori F**. (2003) Influence of dispersive effects on large-signal models based on differential parameter integration. Gallium Arsenide Application Symposium.
15. **Gibiino GP, Santarelli A and Filicori F** (2018) A Procedure for GaN HEMT Charge Functions Extraction from Multi-Bias S-Parameters. European Microwave Integrated Circuits Conference (EuMIC), 65–68.
16. **Niessen D, Gibiino GP, Cignani R, Santarelli A, Schreurs D and Filicori F**. (2016) Charge-controlled GaN FET modeling by displacement current integration from frequency-domain NVNA measurements. *IEEE Transactions on Microwave Theory and Techniques* **64**, 4382–4393.
17. **Goncalves CF, Nunes LC, Cabral PM and Pedro JC** (2018) Pulsed I/V and S-parameters measurement system for isodynamic characterization of power GaN HEMT transistors. *International Journal of RF and Microwave Computer-Aided Engineering* **28**, e21515. https://doi.org/10.1002/mmce.21515

https://doi.org/10.1017/S1759078719000059 Published online by Cambridge University Press

18. **Santarelli A, Cignani R, Niessen D, Traverso P and Filicori F** (2012) New pulsed measurement setup for GaN and GaAs FETs characterization. *International Journal of Microwave and Wireless Technologies* **4**, 387–397.
19. **Santarelli A, Cignani R, Gibiino GP, Niessen D, Traverso PA, Florian C, Schreurs D and Filicori F**. (2014) A double-pulse technique for the dynamic I/V characterization of GaN FETs. *Microwave Components Letters* **24**, 132–134.
20. **Goncalves CF, Nunes LC, Cabral PM and Pedro JC** (2017) Conservative current and charge data extracted from pulsed S-parameter measurements for GaN HEMT PA design. IEEE MTT-S International Microwave Symposium (IMS), 1065–1068.
21. **Jansen P, Schreurs D, De Raedt W, Nauwelaers B and Van Rossum M** (1995) Consistent small-signal and large-signal extraction techniques for heterojunction FET's. *IEEE Transactions on Microwave Theory and Techniques* **43**, 87–93.
22. **Curras-Francos MC, Tasker PJ, Fernandez-Barciela M, Campos-Roca Y and Sanchez E** (2000) Direct extraction of nonlinear FET Q-V functions from time domain large signal measurements. *IEEE Microwave and Guided Wave Letters* **10**, 531–533.
23. **Camacho-Peñalosa C, Martin-Guerrero TM and Baños-Polglase JD** (2006) Frequency domain-based extraction method of quasi-static non-linear state functions from large-signal measurements. *Microwave and Optical Technology Letters* **1**, 90–99.
24. **Martin-Guerrero TM, Baños-Polglase JD, Camacho-Peñalosa C, Fernandez-Barciela M, Morgan DG and Tasker PJ** (2006) Frequency domain based approach for nonlinear quasi-static FET model extraction from large-signal waveform measurements. European Microwave Integrated Circuits Conference (EuMIC), 441–444.
25. **Perez-Parras S, Martin-Guerrero TM, Baños-Polglase JD and Camacho-Peñalosa C** (2018) Frequency Domain-Based Method for a Two-Port Nonlinear Quasi-Static Model Extraction from Large-Signal Waveforms. European Microwave Integrated Circuits Conference (EuMIC), 69–72.
26. **Niessen D, Gibiino GP, Cignani R, Santarelli A, Schreurs D and Filicori F** (2016) Iso-thermal and iso-dynamic direct charge function characterization of GaN FET with single large-signal measurement. IEEE MTT-S International Microwave Symposium (IMS), 1–3.
27. **D'Errico J** (2005) Surface fitting using gridfit. MATLAB central file exchange 643 [online].
28. **Dambrine G, Cappy A, Heliodore F and Playez E** (1988) A new method for determining the FET small-signal equivalent circuit. *IEEE Transactions on Microwave Theory and Techniques* **36**, 1151–1159.
29. **Gibiino GP, Santarelli A and Filicori F** (2018) A GaN HEMT global large-signal model including charge trapping for multibias operation. *IEEE Transactions on Microwave Theory and Techniques* **66**, 4684–4697.
30. **Florian C, Santarelli A, Cignani R and Filicori F** (2013) Characterization of the nonlinear thermal resistance and pulsed thermal dynamic behavior of AlGaN-GaN HEMTs on SiC. *IEEE Transactions on Microwave Theory and Techniques* **61**, 1879–1891.



Gian Piero Gibiino received the dual Ph.D. degree from the University of Bologna, Bologna, Italy, and KU Leuven, Leuven, Belgium, in 2016. Since 2012, he has been with the Department of Electrical, Electronic, and Information Engineering "Guglielmo Marconi" (DEI), University of Bologna, where he is currently a Post-Doctoral Research Fellow. In 2016, he was a Visiting Researcher with Keysight Technologies, Aalborg, Denmark. His current research interests include the characterization and empirical modeling of microwave devices and systems, microwave measurements, and RF instrumentation.



Alberto Santarelli received the Laurea degree (cum laude) in electronic engineering in 1991 and the Ph.D. in Electronics and Computer Science from the University of Bologna, Italy in 1996. He was a Research Assistant from 1996 to 2001 with the Research Centre for Computer Science and Communication Systems of the Italian National Research Council (IEIIT-CNR) in Bologna. In 2001, he joined the Department of Electrical, Electronic and Information Engineering "Guglielmo Marconi" (DEI), University of Bologna, where he is currently an Associate Professor. During his academic career he has been a Lecturer of Applied Electronics, High-frequency Electronics and Power Electronics. His main research interests are related to the nonlinear characterization and modeling of electron devices and to the nonlinear microwave circuit design.



Fabio Filicori received the M.S. degree in electronic engineering from the University of Bologna, Bologna, Italy, in 1974. In the same year he joined the Department of Electronics, Computer Science and Systems, University of Bologna, initially as Research Assistant, and then as an Associate Professor. In 1990 he became Full Professor with the University of Perugia, Perugia, Italy. In 1991 he joined the University of Ferrara, Ferrara, Italy. In 1993, he joined again the University of Bologna. He has been a member of the Space Technology Committee of the Italian Space Agency and responsible for several research projects for the Italian National Research Council. He was TPC chair of the EuMIC conference in 2009. During his academic career, he has held courses on CAD, electron devices and circuits, and power electronics. His main research activities are in the areas of CAD techniques for nonlinear microwave circuits, electron device nonlinear modeling, sampling digital instrumentation and power electronics. After retiring in 2016, he is still involved in teaching and research activities at the University of Bologna as an adjunct professor.

https://doi.org/10.1017/S1759078719000059 Published online by Cambridge University Press